



Influence of laser shock peening on irradiation defects in austenitic stainless steels



Qiaofeng Lu^a, Qing Su^b, Fei Wang^a, Chenfei Zhang^c, Yongfeng Lu^c, Michael Nastasi^{a, b, d}, Bai Cui^{a, d, *}

^a Department of Mechanical & Materials Engineering, University of Nebraska–Lincoln, Lincoln, NE 68588, USA

^b Nebraska Center for Energy Sciences Research, University of Nebraska–Lincoln, Lincoln, NE 68588, USA

^c Department of Electrical Engineering, University of Nebraska–Lincoln, Lincoln, NE 68588, USA

^d Nebraska Center for Materials and Nanoscience, University of Nebraska–Lincoln, Lincoln, NE 68588, USA

HIGHLIGHTS

- Laser shock peening generates a dislocation network, stacking faults and deformation twins in stainless steels.
- Dislocations and incoherent twin boundaries serve as effective sinks for the annihilation of irradiation defects.
- Incoherent twin boundaries remain as stable and effective defect sinks at 300 °C.

ARTICLE INFO

Article history:

Received 25 July 2016

Received in revised form

16 March 2017

Accepted 29 March 2017

Available online 31 March 2017

Keywords:

Laser shock peening

Irradiation

In-situ TEM

Stainless steel

Microstructure

ABSTRACT

The laser shock peening process can generate a dislocation network, stacking faults, and deformation twins in the near surface of austenitic stainless steels by the interaction of laser-driven shock waves with metals. In-situ transmission electron microscopy (TEM) irradiation studies suggest that these dislocations and incoherent twin boundaries can serve as effective sinks for the annihilation of irradiation defects. As a result, the irradiation resistance is improved as the density of irradiation defects in laser-peened stainless steels is much lower than that in untreated steels. After heating to 300 °C, a portion of the dislocations and stacking faults are annealed out while the deformation twins remain stable, which still provides improved irradiation resistance. These findings have important implications on the role of laser shock peening on the lifetime extension of austenitic stainless steel components in nuclear reactor environments.

© 2017 Elsevier B.V. All rights reserved.

1. Introduction

With a combination of high ductility, strength, and toughness, austenitic stainless steels are widely used in pipelines and steam generators in light water reactors (LWR). However, two vital problems limit the lifetime of austenitic stainless steel structural components in reactor environments, namely, irradiation damage and stress corrosion cracking (SCC) [1–3]. Irradiation of metals with energetic particles, such as neutrons and heavy ions, results in the formation of vacancy- and interstitial-type point defects [4–6]. The accumulation of these point defects could further evolve into defect

clusters, such as dislocation loops [7,8], stacking fault tetrahedra [9], and voids [10] in stainless steels, depending on the irradiation conditions, including the dose level and temperature. These irradiation defects cause significant structural instability and degradation of mechanical properties of stainless steels in the irradiation environment.

The irradiation tolerance of materials can be improved by microstructural modification via introduction of a high density of defect sinks, such as dislocations [11], grain boundaries [12,13], and nanoscale interfaces [14]. It is expected that the irradiation defect clusters will migrate to and be annihilated at these sinks. For example, nanocrystalline metals of tungsten (W), nickel (Ni), and 304L stainless steels exhibit a higher radiation tolerance than their bulk counterparts due to an increased density of grain boundaries [15–17]. Multilayer nanocomposites with immiscible interfaces,

* Corresponding author. Department of Mechanical & Materials Engineering, University of Nebraska–Lincoln, Lincoln, NE 68588, USA.

E-mail address: bcui3@unl.edu (B. Cui).

such as iron/silicon oxycarbide (Fe/SiOC), copper/niobium (Cu/Nb), and vanadium/silver (V/Ag), can effectively mitigate radiation-induced swelling and a loss of mechanical integrity [18–21]. Oxide-dispersion-strengthened (ODS) stainless steels, which have a dispersion of incoherent particle/matrix interfaces, exhibit an enhanced resistance to void swelling and helium bubble embrittlement [22–25].

Laser shock peening (LSP) is a novel surface modification approach that can mitigate most types of failures of metallic materials, such as fatigue, wear, and SCC [26,27]. In the LSP process, a laser beam hits the sacrificial coating on the surface of the metal target and forms a plasma, which rapidly expands and generates shock waves into the bulk (Fig. 1). The laser-driven shock waves cause significant compressive residual stresses (typically 0.1–1 GPa) that can extend to a depth of more than 1 mm from the surface [28,29]. Compared to traditional mechanical shot peening, LSP offers many advantages, such as deeper penetration of compressive stresses (typically > 1 mm, which is about ten times that of mechanical shot peening), shorter process times (typically several tens of nanoseconds), precise control, accuracy, and flexibility [30,31]. For example, LSP has succeeded in improving the fatigue life of metal components of aircraft structures and engines by General Electric Infrastructure-Aviation and LSP Technologies [32,33]. Recently, there have been a few successful studies that employ LSP to prevent SCC of austenitic stainless steels [34–36]. The improvement of SCC resistance by LSP has been generally attributed to the effect of compressive residual stresses and microstructural changes, although the exact mechanistic mechanism has not been well elucidated [35].

Experimental investigations have revealed that the benefit of LSP is related to the microstructural evolution near the surface of materials during the LSP process. The interaction of laser-driven shock waves with metallic materials causes severe plastic deformation, which can manifest as dislocation networks, deformation twins, and grain refinement [37–39]. Highly tangled and dense dislocations and dislocation-cell structures are observed in aluminum alloys subjected to LSP [38,40]. Grain refinement is observed in 304 stainless steels with the grain size increasing with depth, the mechanism of which is suggested to be caused by twin-twin intersections, which transform to subgrain boundaries [35,37,41]. To our knowledge, no previous research studied the effects of LSP on the irradiation resistance of materials. However, we hypothesize that the modified microstructure on the surface of austenitic stainless steels will change their response to the irradiation damage.

The objective of the research documented by this paper is to determine if LSP can improve the irradiation resistance of austenitic stainless steels. The microstructural evolution of austenitic stainless steels during the LSP process was studied using transmission

electron microscopy (TEM). The irradiation behavior of laser-peened austenitic stainless steels was investigated using in-situ TEM irradiation experiments at the intermediate voltage electron microscope (IVEM)-Tandem facility at the Argonne National Laboratory to directly observe the dynamics of interactions of irradiation defects with potential sinks, such as dislocations and twin boundaries. The thermal stability of as-formed microstructures was also observed by in-situ TEM heating experiments from room temperature to 300 °C, which is around the operating temperature of LWR. These findings have important implications on the lifetime extension of austenitic stainless steel components in nuclear reactors by LSP. That is, in addition to its well-known effect of preventing fatigue and SCC, LSP may also improve the irradiation resistance of austenitic stainless steels.

2. Material and methods

Commercial purity 304 stainless steels (Fe-18.3% Cr-8.5% Ni-1.38% Mn-0.65% Si-0.03% S-0.04% C by weight) were used as model materials in this study. The static yield strength is 290 MPa. The sample was annealed at 950 °C for 30 min under Ar atmosphere. The initial microstructural characterization showed a grain size of 25–50 μm, a low dislocation density and no precipitates.

In the LSP experiments, the geometrical dimensions of samples were 10 mm × 8 mm × 2 mm, which were cut using a diamond saw. The samples were ground using silicon carbide (SiC) grinding papers, followed by polishing using 3 μm and 0.3 μm alumina powders. LSP was performed using a Q-switched Nd:YAG laser source at room temperature. Typical parameters of the LSP process, such as the laser pulse energy, laser pulse number, spot diameter, pulse duration, and overlap ratio are listed in Table 1. The magnitude and depth of compressive residual stress generated by LSP is increased with the laser energy and the number of LSP scans [36,42]. Therefore, the highest laser energy in the Nd:YAG laser (850 mJ) was chosen in this study and the sample was treated by LSP for 5 times. Scanning the laser beam can enable LSP on an area of 10 mm × 8 mm of the 304 stainless steel samples. The sample surface was coated with a 177 μm thick black tape as a sacrificial layer to avoid laser ablation. A flowing film of deionized water covered the sample surface, which acted as the plasma-confining media [27,34]. It is important to note that in this LSP process, the metal samples remained at room temperature with the protection of the sacrificial layer and the water film.

3. Experimental

The near-surface microstructure of 304 stainless steels was characterized by transmission electron microscopy (TEM) after the LSP process. The specimens were cut from the region close to the surface and thinned to a thickness of less than 100 μm by mechanical polishing. Final thinning to electron transparency was performed using a twin jet polisher with a 5% perchloric acid and 95% methanol electrolyte at –20 °C. Assuming the electropolishing

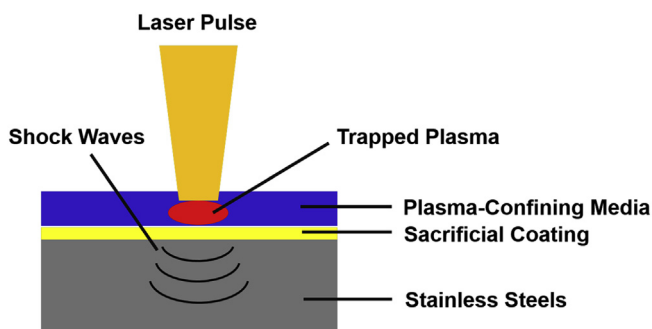


Fig. 1. Schematic of the LSP process of stainless steels.

Table 1

Typical experimental parameters for LSP of austenitic stainless steels.

Pulse energy (mJ)	850
Spot diameter (mm)	1
Pulse duration (ns)	7
Number of LSP scans	5
Overlap ratio	50%
Repetition-rate (Hz)	10
Laser wavelength (nm)	1064
Beam profile	Gaussian

removes approximately the same thickness from two sides, the region for TEM observation could be estimated to be about 50 μm from the top surface. TEM was carried out in a JEOL 2010 LaB₆ operated at 200 kV. Microstructures were examined in the TEM using diffraction-contrast bright-field (BF) and weak-beam dark-field (WBDF) imaging modes. The Burgers vector of the dislocations was determined by using the $\mathbf{g}\cdot\mathbf{b}$ invisibility condition. Selected area electron diffraction (SAED) was used for crystallographic analysis.

The in-situ TEM experiments were performed at the IVEM-Tandem microscope facility. This facility consists of a Hitachi 9000 TEM and an ion accelerator. The TEM samples were irradiated with Kr⁺ at 1 MeV to an influence of up to 3×10^{18} ions m^{-2} , which was estimated to be equivalent to 1.33 dpa in a 100 nm-thick foil, calculated using the Stopping and Range of Ions in Matter (SRIM) simulation code [43]. The dose rate was 0.00167 dpa/s. Two different temperature conditions were used: one was at room temperature and the other was at 300 °C. Under these irradiation conditions, the irradiation-induced defect clusters in austenitic stainless steel were dislocation loops [7,44]. The areal density of dislocation loops was calculated as a function of irradiation dose and temperature, which is defined as the number of dislocation loops in a unit area of the TEM foil. The procedures for counting the numbers and errors of dislocation loops followed the method described by Kirk and Jenkins [45]. The in-situ irradiation and heating experiments were accomplished using a double-tilt heat stage (Gatan model 652, Gatan Inc., Warrendale, PA). The dynamic process of the microstructural evolution during irradiation and heating was recorded as videos using a charge-coupled device (CCD) camera with a recording rate of 10 frames per second. The recorded videos were combined with conventional micrographs to determine the sequence of the annihilation process of the irradiation defects.

4. Results

4.1. TEM observation of the near-surface microstructure of laser-peened 304 steels

Fig. 2 shows the typical microstructures, such as deformation

twins, stacking faults, and dislocation network, in the near-surface region (about 50 μm in depth) of laser-peened 304 stainless steels. The width of deformation twins ranged from 30 nm to 200 nm, and the twin density was $(1.98 \pm 0.36) \times 10^{10} \text{ m}^{-2}$. There are two types of twin boundary in the microstructures of laser-peened 304 steels: coherent twin boundary (CTB) and incoherent twin boundary (ITB). The CTB is $\sum 3\langle 111 \rangle / 60^\circ$, in which the rotation axis is $\langle 111 \rangle$ and the rotation angle is 60° . The ITB is $\sum 3\langle 101 \rangle / 70.5^\circ$, in which the rotation axis is $\langle 101 \rangle$ and the rotation angle is 70.5° . The CTB has a perfect atomic fit (coherency) in the boundary and lowest energy, while the ITB has less atomic fit and higher energy than the ITB.

The dislocation density of laser-peened samples was $(9.63 \pm 1.24) \times 10^{13} \text{ m}^{-2}$, which was more than one order of magnitude larger than the dislocation density of untreated samples $[(6.53 \pm 0.85) \times 10^{12} \text{ m}^{-2}]$. The Burgers vectors of these dislocations were in the family of $\frac{1}{2}\langle 110 \rangle$. The stacking fault ribbons (Fig. 2c and d) were bounded by a pair of partial dislocations with a Burgers vector of $\frac{1}{6}\langle 112 \rangle$, which were formed by the dissociation of perfect dislocations with a Burgers vector of $\frac{1}{2}\langle 110 \rangle$. It is noted that the 304 stainless steels had a low stacking fault energy (15–20 mJ m^{-2}), which allowed for easy formation of stacking faults during plastic deformation [46]. The stacking fault energy of this 304 steel sample was calculated to be 16.6 mJ/m^2 by measuring the separation between partial dislocations [47].

The presence of deformation twins, stacking faults, and dislocation network suggests that significant plastic deformation occurred in the 304 stainless steels during the LSP process. During LSP, the laser-driven shock waves propagate into the metals and generate a high magnitude of shock-induced pressure (typically several GPa) [48]. The pressure of the shock wave exceeds the dynamic yield strength of 304 stainless steels ($\sim 210 \text{ MPa}$ [49]), which experience an extremely high strain rate ($10^6\text{--}10^8 \text{ s}^{-1}$) during a short period of time (several tens of nanoseconds) [28]. The shock wave pressure is thus the origin of the plastic deformation in the near-surface of the alloy. Many studies in the literature have simulated the dynamic response of metals subjected to LSP using the finite element method [29,50,51]. It is also important to note that the compressive stress and plastic deformation generated by LSP decrease with the depth of the sample [34,35]. In addition, LSP increased the hardness of 304 steel due to the significant plastic

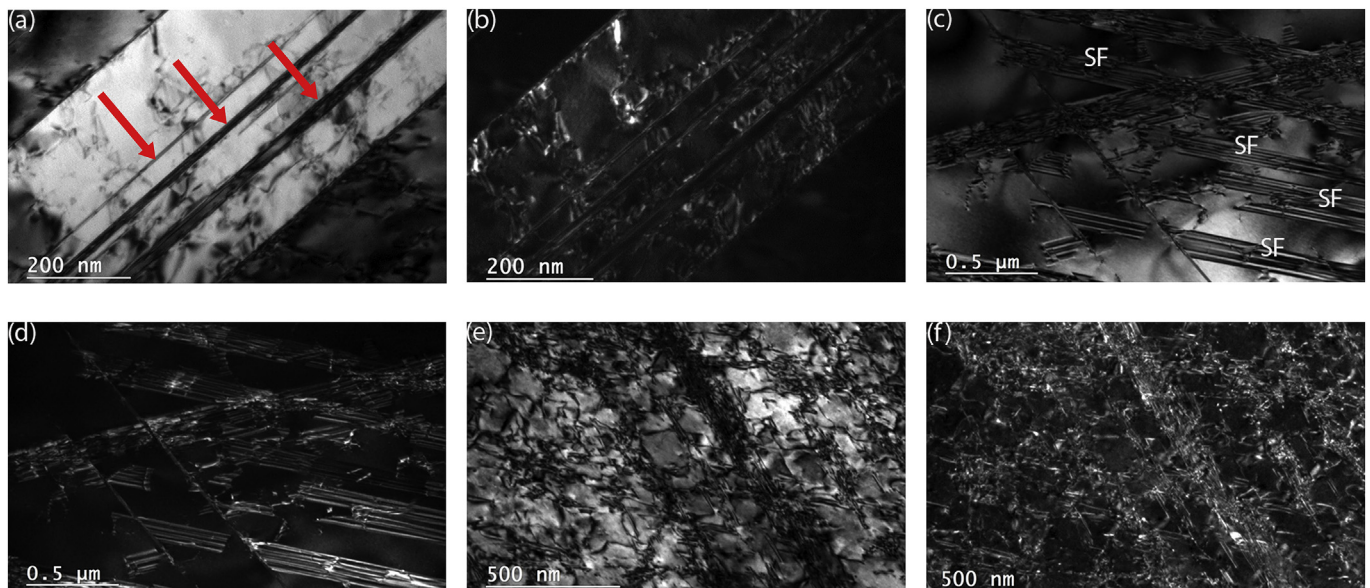


Fig. 2. Typical TEM images of the near-surface microstructures of 304 austenitic stainless steel treated by LSP: (a, b) deformation twins (arrowed); (c, d) stacking faults (SF); and (e, f) dislocation network. a, c and e are BF images; b, d and f are the corresponding WBDF images.

deformation; the hardness decreases with the depth of samples.

To study the microstructural changes of laser-peened 304 stainless steels at elevated temperatures, the samples were heated in-situ to 300 °C inside the TEM chamber. The typical LWR operating temperature is around 300 °C [1]. During the heating process, some dislocations disappeared due to the effect of thermal annealing; and some stacking faults disappeared due to the recombination of the pair of partial dislocations with a Burgers vector of $\frac{1}{6}\langle 112 \rangle$ to an extended dislocation with a Burgers vector of $\frac{1}{2}\langle 110 \rangle$. The twin boundaries were unchanged during the heating, and no grain growth was observed. Fig. 3 shows the same region (an area of 1.3 μm^2) before and after heating to 300 °C for about 10 min. It was observed that the disappearance of most dislocations and stacking faults occurred during the heating process, from 25 to 300 °C, not during the annealing at 300 °C. The dislocation density of this region was slightly reduced from $(9.14 \pm 1.02) \times 10^{13} \text{ m}^{-2}$ at 25 °C to $(6.42 \pm 0.77) \times 10^{13} \text{ m}^{-2}$ at 300 °C.

4.2. Irradiation damage of laser-peened 304 stainless steels

Under 1 MeV Kr^+ irradiation in the temperature regime of 25–300 °C, the dominant irradiation defect clusters in the 304 stainless steel samples are dislocation loops (<10 nm) [7]. It has been well documented that the irradiation-induced defects in austenitic stainless steel are dislocation loops [7,44,52–54]. The dislocation loops are predominantly interstitial-type Frank (faulted) loops ($\mathbf{b} = 1/3\langle 111 \rangle$) due to high diffusivity of interstitials at low temperatures [7,55]. LSP does not change the type of irradiation defect clusters. These dislocation loops appear as bright dots under the WBDF imaging conditions in TEM.

The regions with the following microstructural features in laser-peened 304 stainless steel samples were selected for in-situ irradiation experiments: a region with a dislocation network and another region with deformation twin boundaries. During the irradiation process, videos were recorded in these regions to observe the dynamic processes of nucleation, growth, mitigation, and annihilation of irradiation defect clusters. The relationship of the dislocation loop density as a function of irradiation dose was determined through the quantitative analysis of snapshots of the videos. A similar analysis was carried out for the irradiation of the samples at 25 and 300 °C.

Fig. 4 shows a typical example of the annihilation process of a dislocation loop by a dislocation line at 25 °C. This dislocation loop nucleated in the vicinity of the dislocation line (Fig. 4a) and gradually grew up with more irradiation defects joining in during the Kr^+ irradiation (Fig. 4b). However, it was annihilated by the dislocation line after 95 s. The Burgers vector of this dislocation loop was

not determined. However, under the environment of Kr^+ irradiation and 25–300 °C, the dislocation loop in 304 stainless steels was most likely a Frank loop with a Burgers vector of $\frac{1}{3}\langle 111 \rangle$ [7,56]. A large number of similar events of the annihilation of dislocation loops by dislocation lines was observed in laser-peened 304 stainless steel samples at both 25 and 300 °C. Although a lower density of dislocations was observed in the laser-peened samples at 300 °C, the dislocations were still found to be effective sinks for the annihilation of irradiation defects.

Fig. 5 shows a typical example of the annihilation process of dislocation loops by an ITB at 25 °C. The rotation angle of this ITB is measured as 68.1° using the electron diffraction. It has a deviation angle of 2.4° from the standard ITB $\Sigma 3\langle 101 \rangle/70.5^\circ$ which has a rotation angle of 70.5°. In this case, two dislocation loops were nucleated in the vicinity of the twin boundary, nearly at the same time (Fig. 5a). Dislocation loop 1 was first annihilated by the twin boundary at 4 s (Fig. 5b); and later, dislocation loop 2 was annihilated at 32 s (Fig. 5c). The reasons for the different annihilation times of dislocation loops 1 and 2 could be related to the differences in the number of point defects in each loop and in the localized structure of the twin boundary. Similar annihilations of dislocation loops by ITBs were also observed in laser-peened 304 stainless steel samples at both 25 °C and 300 °C, which suggested that the ITB is another type of irradiation defect sink.

The evolution of dislocation loop density as a function of irradiation dose was determined at 25 and 300 °C in the laser-peened 304 steels and compared with untreated 304 steels under the same irradiation conditions.

In the region with a dislocation network at 25 °C, the density of dislocation loops increased with the irradiation dose and appeared to saturate at a dose level of $2.25 \times 10^{18} \text{ ions/m}^2$ (~1 dpa) (Fig. 6a), which is lower than the regular (untreated) 304 steels (~5 dpa [57]). Compared with untreated 304 steels under the same irradiation conditions, the laser-peened 304 steels show a much lower density of dislocation loops at the same dose level (Fig. 6a). These results suggest that LSP improves the irradiation resistance of 304 steels by providing dislocations as the sinks for the annihilation of irradiation defects. At 300 °C, the density of dislocation loops in dislocation network regions showed an increase compared to that at 25 °C. This may be explained by the slight reduction of the dislocation density from $(9.14 \pm 1.02) \times 10^{13} \text{ m}^{-2}$ at 25 °C to $(6.42 \pm 0.77) \times 10^{13} \text{ m}^{-2}$ at 300 °C. Another possible reason is that increasing the temperature can promote the diffusion of interstitials, allowing them to escape to defect sinks, such as dislocations, leaving vacancies behind to cluster [58,59]. The density of vacancy-type dislocation loops is thus increased at higher temperatures because there are less interstitials to recombine and

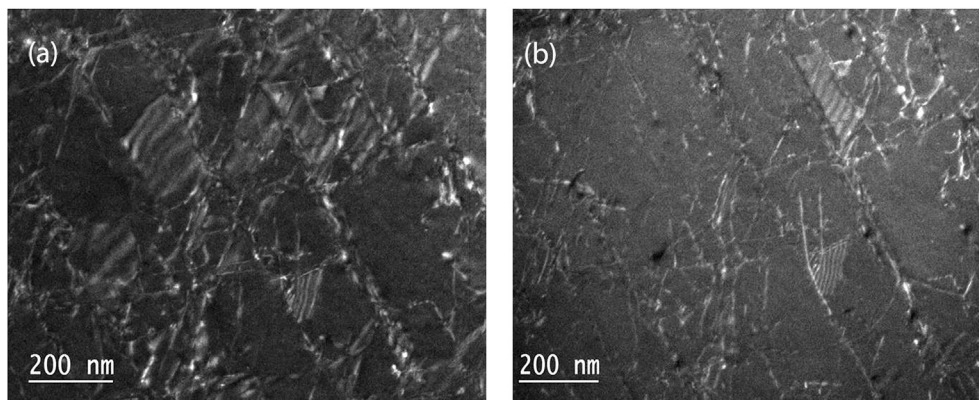


Fig. 3. TEM images of the laser-peened 304 steel samples: (a) at room temperature and (b) after heating to 300 °C.

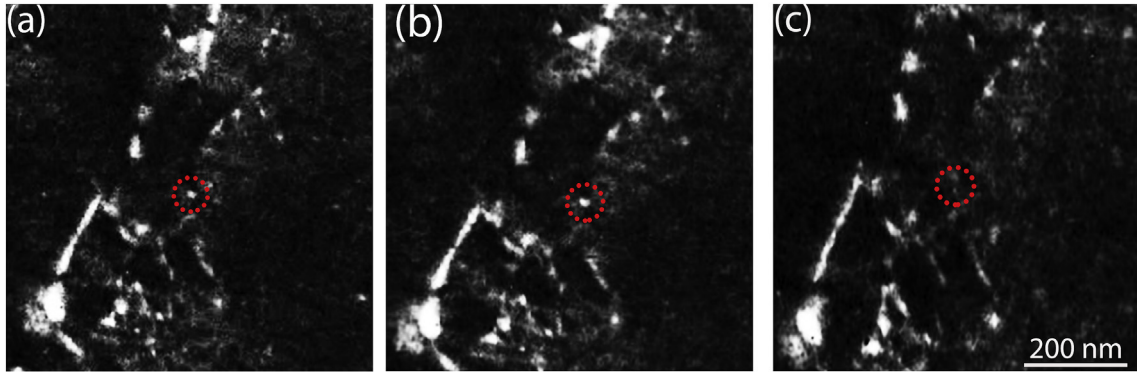


Fig. 4. Annihilation process of a dislocation loop by a dislocation line in a laser-peened 304 steel sample under 1 MeV Kr⁺ irradiation and 25 °C. The snapshots show the dislocation loops (bright spot in the circle) (a) formed at 0 s, (b) growing up at 19 s, and (c) annihilated by the dislocation line at 95 s.

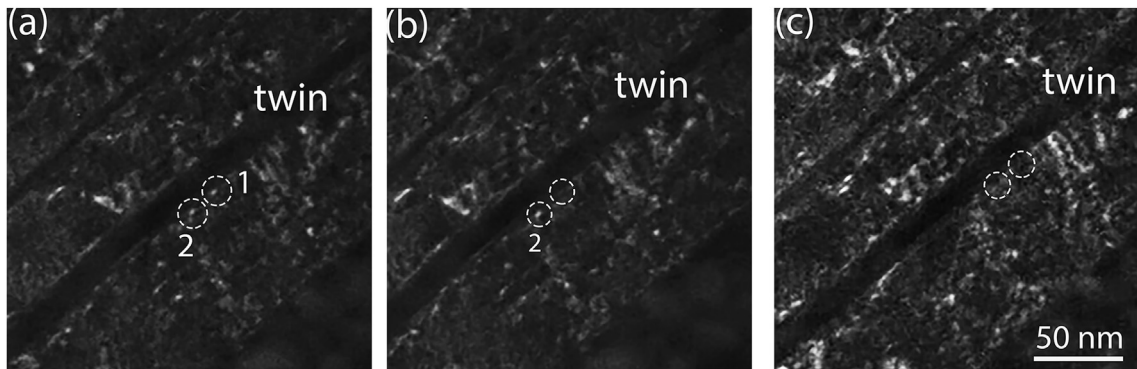


Fig. 5. Annihilation process of dislocation loops by an incoherent twin boundary ($\Sigma 3[101]/68.1^\circ$) in a laser-peened 304 steel sample under 1 MeV Kr⁺ irradiation and 25 °C: (a) two dislocation loops (1 and 2) (bright spots in circles) formed at 0 s; (b) Loop 1 was annihilated at 4 s; and (c) Loop 2 was annihilated at 32 s.

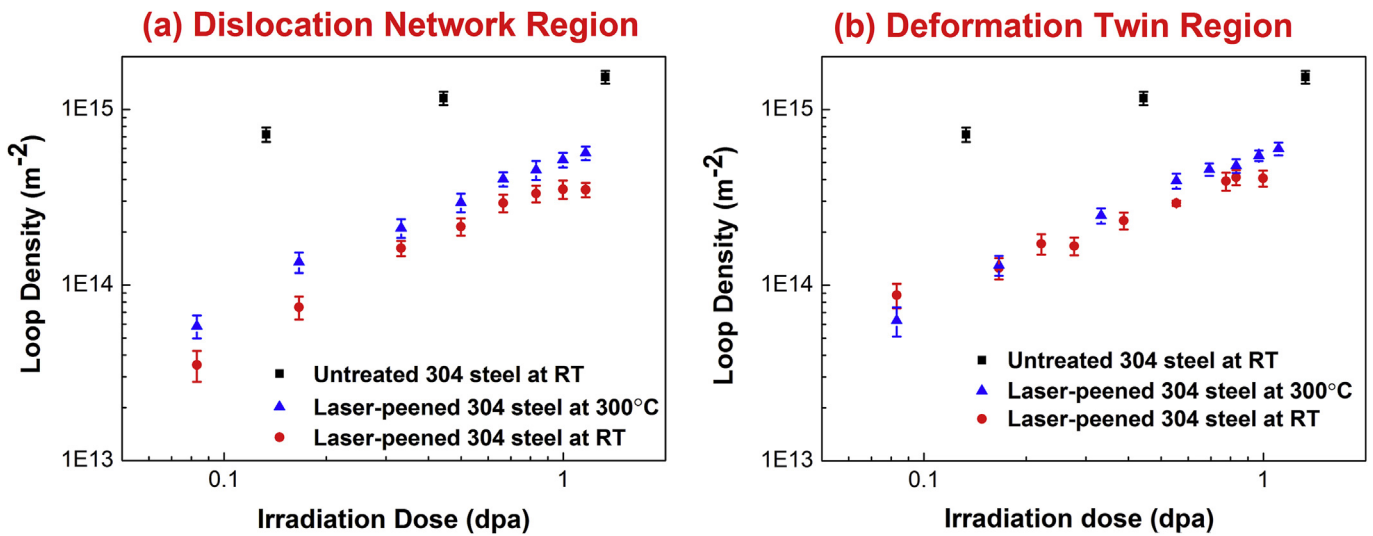


Fig. 6. The density of dislocation loops as a function of irradiation dose under 1 MeV Kr⁺ irradiation in the region of: (a) dislocation network in laser-peened 304 stainless steels at room temperature (RT) and 300 °C and (b) deformation twins in laser-peened 304 steels at RT and 300 °C. These are compared with untreated 304 stainless steel samples at RT.

annihilate with vacancies.

In the region with deformation twins at 25 °C, the density of dislocation loops also increased with the irradiation dose and saturated at approximately the dose level of 1.875×10^{18} ions/m² (~0.83 dpa) (Fig. 6b). The density of dislocation loops in the region of deformation twins in laser-peened 304 steels was much lower

compared with untreated 304 steels at the same dose level (Fig. 6b). This is due to the fact that ITBs have a higher energy than CTBs and can act as the sinks for the annihilation of irradiation defects, which will be further discussed in Section 5. Compared to the dislocation network region (Fig. 6a), the density of dislocation loops in twin regions had smaller differences between 25 and 300 °C (Fig. 6b).

This may be due to the fact that the ITB can provide “interstitial emission” to react with vacancies near the boundary [13,60]. This “interstitial emission” mechanism will be further discussed later. It is also important to note that the twin boundaries were stable on heating from 25 to 300 °C.

5. Discussion

The mechanisms of defect annihilation by sinks have been studied extensively by in-situ TEM ion irradiation experiments and molecular dynamic (MD) simulations. The stress field of dislocations can interact with irradiation-induced point defects, which causes an interaction energy, E_I , to change the elastic energy of the materials [47]. The point defects migrate into the core region of dislocations to reduce E_I . For example, the interstitials migrate to the tensile strain region below the extra half-plane of an edge dislocation. It is suggested that the interaction between a dislocation and an interstitial is stronger than that between a dislocation and a vacancy [61,62]. Thus, the interstitials preferentially drift to dislocations, allowing excess vacancies to accumulate as void-type clusters. Singh et al. developed a concept of “stand-off distance” for the interaction of dislocations with point defects in the “cascade-induced source hardening” model [63]. The defect clusters that approach dislocation cores within the “stand-off distance” will be absorbed, while clusters can accumulate just outside this distance [11,64]. The value of “stand-off distance” would need to be determined by atomic calculations. However, its lower bound is estimated to be on the order of the size of dislocation loops, i.e., the distance at which a loop is close to touching the dislocation [63,65]. In this study, the average radius of an irradiation-induced loop is around 5 nm, which indicated the “stand-off distance” of dislocations in laser-peened 304 stainless steels. Experimentally, the absorption of defect clusters by dislocations has been frequently observed in many metals under irradiation conditions [65–67]. For example, Rabach et al. found that screw dislocations are more efficient than edge dislocations at annihilating point defects in Kr⁺-irradiated Cu [68].

The sink strength was introduced in the kinetic rate theory which is defined as the loss rate of vacancies or interstitials to a particular type of defect sink [69,70]. The sink strength of a straight dislocation, S_d , can be determined by Refs. [70,71]:

$$S_d = Z_d \rho_d, \quad (1)$$

where ρ_d is the dislocation density, and Z_d is the dislocation capture efficiency of each dislocation. Z_d can be calculated by Ref. [70]:

$$Z_d = \frac{2\pi}{\ln(R_L/R_d)}, \quad (2)$$

where R_d is the dislocation capture radius for point defects, and R_L is dislocation spacing:

$$R_L = (\pi \rho_d)^{-\frac{1}{2}} \quad (3)$$

Note that the terms “dislocation capture radius” and “stand-off distance” originated from different theories but have a similar physic meaning. Thus, if the value of “stand-off distance” (~5 nm) is taken for an estimation of the “dislocation capture radius,” the sink strength of the dislocation in laser-peened 304 stainless steels can be calculated as $(2.47 \pm 0.24) \times 10^{14} \text{ m}^{-2}$ while that for the untreated sample can be calculated as $(1.08 \pm 0.11) \times 10^{13} \text{ m}^{-2}$.

Experimental results in Fig. 6b suggest ITBs are effective sinks for annihilation of irradiation defects in 304 stainless steels, and the sink strength of the ITB is nearly as effective at 300 °C as 25 °C.

Atomistic MD simulations revealed that twin boundaries have complicated interactions with irradiation-induced point defects in face-centered-cubic (FCC) metals. It is generally suggested that twin boundaries can absorb point defects and preferentially absorb interstitials over vacancies [72,73]. King and Smith show that the self-interstitial clusters can grow, coalesce, annihilate, and then re-nucleate on the twin boundary plane in Cu and Al [74]. As a consequence of the formation of these self-interstitial clusters, Mendeleev and King suggest that twin boundaries can become non-saturating sinks for self-interstitials [75]. Specifically, ITBs are more effective sinks than CTBs. Li et al. found that the $\Sigma\{112\}$ ITB in Cu films has preferred sites for adsorbing interstitials under Cu³⁺ ion irradiation [76]. Han et al. investigated the dependence of void-denuded zones (VDZs) on grain boundary character in Cu under 200 keV He irradiation at 450 °C [12]. No obvious VDZs was close to CTB, while a VDZ with a width of 28 nm formed close to ITB. These indicate that ITB has the ability to absorb vacancies and produce a void-free zone near it, suggesting the ITB has a higher sink efficiency than CTB. In this study, the ITB in Fig. 5 has a deviation angle of 2.4° from the standard ITB $\Sigma 3\{101\}/70.5^\circ$. The sink efficiency of the grain boundary is dependent on the density and types of point defect trapping sites, such as jogs, steps or disclinations [12]. The deviation from the standard boundary could increase these point defect trapping sites and thus increase the sink efficiency of ITB.

Because of the biased absorption of interstitials, ITB contain a significantly large concentration of interstitial defects after interaction with the cascade. This leaves behind excess vacancies, which promotes the formation of vacancy clusters within the grain interior. Recently, an “interstitial emission” mechanism was proposed which suggests that the excess interstitials at the grain boundaries can interact strongly with nearby vacancies, leading to enhanced annihilation of vacancies [13,72,78]. Bai et al. found that the interstitial-loaded boundary in Cu can act as an interstitial source, emitting interstitials via a displacement process, with a chain of atoms pushing from the grain boundary to anneal vacancies that are several atomic planes away from the boundary [13]. This interstitial emission process has a much lower energy barrier than that for vacancy migration to the boundary. Later, Chen et al. found that defect-boundary interactions in α -Fe are mediated by chain-like defects which consist of alternately positioned interstitials and vacancies [60]. Through localized recombination of neighboring interstitial-vacancy pairs along the chain, a point defect can be translated from one end to the other end of the chain to annihilate with its opposite defect. The above mechanisms may accelerate the annihilation of less-mobile vacancies in the nearby bulk, which thus cause grain boundaries to act as efficient sinks for both interstitials and vacancies. Because ITBs are specific grain boundaries, this “interstitial emission” mechanism must also be considered when determining the sink efficiency of ITBs. The small difference in the density of dislocation loops in twin regions at 25 and 300 °C (Fig. 6b) may be explained by that the rate of “interstitial emission” is not significantly changed from 25 to 300 °C. However, a comparison between ITBs and the random grain boundary should be based on the sink strength and the free energy in them. These factors need to be taken into account while extending “interstitial emission” mechanism.

Finally, this study showed that LSP is a promising engineering approach in improving the irradiation resistance of stainless steels at a dose up to 1.3 dpa at 25–300 °C. This is due to the formation of a dislocation network and ITBs induced by LSP, which serve as effective sinks for annihilation of irradiation defects. In particular, different from the dislocations which can be annealed by elevated temperature, the ITBs remained as stable and effective sinks at 300 °C. However, under the current experimental conditions (Table 1), the LSP effects were limited to a depth of about 1 mm

from the surface, which is the penetration distance of laser-driven shock waves. Therefore, the improvement of irradiation resistance in the current study was limited to about 1 mm depth from the surface. Future work will focus on improving the LSP process by changing the processing parameters to increase the depth of LSP effects and promote the formation of nanoscale deformation twins.

6. Conclusions

1. The laser-driven shock waves in the LSP process can produce severe plastic deformation in austenitic stainless steels. Dislocation network, stacking faults, and deformation twins were generated in the near-surface region of laser-peened 304 stainless steels. After heating to 300 °C, the density of dislocations and stacking faults was reduced while the deformation twins remained stable.
2. The dislocation network and ITBs can serve as high strength sinks for the annihilation of irradiation defects during the heavy ion irradiation, although they have different interaction mechanisms with interstitial- and vacancy-type defects. The defect density in laser-peened 304 stainless steels was much lower than that in untreated steels. Consequently, the LSP process can improve the radiation resistance of stainless steels at 25 and 300 °C by introducing defect sinks.

Acknowledgements

This work was supported by the Nebraska Public Power District through the Nebraska Center for Energy Sciences Research, Research Council Faculty Seed Grant from the University of Nebraska-Lincoln, and the Department of Energy (DOE) Office of Nuclear Energy, Nuclear Energy Enabling Technologies [grant number DE-NE0000533]. The electron microscopy with in-situ ion irradiation was accomplished at Argonne National Laboratory at the IVEM-Tandem facility, a U.S. DOE facility funded by the DOE Office of Nuclear Energy, operating under Contract No. DE-AC02-06CH11357 by UChicago Argonne, LLC. The authors would like to express their great gratitude to Mark Kirk, Peter M. Baldo, Edward A. Ryan, and Meimei Li for their help with the operation of this facility. The research was performed in part in the Nebraska Nanoscale Facility: National Nanotechnology Coordinated Infrastructure and the Nebraska Center for Materials and Nanoscience, which are supported by the National Science Foundation under Award ECCS 1542182 and the Nebraska Research Initiative.

References

- [1] S.J. Zinkle, G. Was, Materials challenges in nuclear energy, *Acta Mater.* 61 (3) (2013) 735–758.
- [2] K. Fukuya, Current understanding of radiation-induced degradation in light water reactor structural materials, *J. Nucl. Sci. Technol.* 50 (3) (2013) 213–254.
- [3] B. Cui, M.D. McMurtrey, G.S. Was, I.M. Robertson, Micromechanistic origin of irradiation-assisted stress corrosion cracking, *Philos. Mag.* 94 (36) (2014) 1–22.
- [4] H. Sakaida, N. Sekimura, S. Ishino, In-situ observation of cascade damage in nickel and copper under heavy ion irradiation, *J. Nucl. Mater.* 179 (1991) 928–930.
- [5] N. Sekimura, S. Ishino, Stability of cascade clusters in gold under energetic heavy ion irradiation, *J. Nucl. Mater.* 155 (1988) 1217–1221.
- [6] H. Abe, N. Sekimura, T. Tadokoro, Stability and mobility of interstitial-type defect clusters generated from displacement cascades in copper and gold by in-situ transmission electron microscopy, *Mater. Trans.* 46 (3) (2005) 433–439.
- [7] J.I. Cole, S.M. Bruemmer, Post-irradiation deformation characteristics of heavy-ion irradiated 304L SS, *J. Nucl. Mater.* 225 (1995) 53–58.
- [8] N. Hashimoto, S. Zinkle, A. Rowcliffe, J. Robertson, S. Jitsukawa, Deformation mechanisms in 316 stainless steel irradiated at 60 C and 330 C, *J. Nucl. Mater.* 283 (2000) 528–534.
- [9] R. Schibli, R. Schäublin, On the formation of stacking fault tetrahedra in irradiated austenitic stainless steels—A literature review, *J. Nucl. Mater.* 442 (1) (2013) S761–S767.
- [10] C. Pokor, Y. Brechet, P. Dubuisson, J.-P. Massoud, A. Barbu, Irradiation damage in 304 and 316 stainless steels: experimental investigation and modeling. Part I: evolution of the microstructure, *J. Nucl. Mater.* 326 (1) (2004) 19–29.
- [11] N. Ghoniem, B. Singh, L. Sun, T.D. de la Rubia, Interaction and accumulation of glissile defect clusters near dislocations, *J. Nucl. Mater.* 276 (1) (2000) 166–177.
- [12] W. Han, M. Demkowicz, E. Fu, Y. Wang, A. Misra, Effect of grain boundary character on sink efficiency, *Acta Mater.* 60 (18) (2012) 6341–6351.
- [13] X.-M. Bai, A.F. Voter, R.G. Hoagland, M. Nastasi, B.P. Uberuaga, Efficient annealing of radiation damage near grain boundaries via interstitial emission, *Science* 327 (5973) (2010) 1631–1634.
- [14] B.P. Uberuaga, S. Choudhury, A. Caro, Ideal sinks are not always ideal: radiation damage accumulation in nanocomposites, *J. Nucl. Mater.* 462 (2015) 402–408.
- [15] C. Sun, M. Song, K. Yu, Y. Chen, M. Kirk, M. Li, H. Wang, X. Zhang, In situ evidence of defect cluster absorption by grain boundaries in Kr ion irradiated nanocrystalline Ni, *Metallurgical Mater. Trans. A* 44 (4) (2013) 1966–1974.
- [16] C. Sun, S. Zheng, C. Wei, Y. Wu, L. Shao, Y. Yang, K. Hartwig, S. Maloy, S. Zinkle, T. Allen, Superior radiation-resistant nanoengineered austenitic 304L stainless steel for applications in extreme radiation environments, *Sci. Rep.* 5 (2015).
- [17] O. El-Atwani, A. Suslova, T. Novakowski, K. Hattar, M. Efe, S. Harilal, A. Hassanein, In-situ TEM/heavy ion irradiation on ultrafine- and nanocrystalline-grained tungsten: effect of 3MeV Si, Cu and W ions, *Mater. Charact.* 99 (2015) 68–76.
- [18] M. Demkowicz, R. Hoagland, J. Hirth, Interface structure and radiation damage resistance in Cu-Nb multilayer nanocomposites, *Phys. Rev. Lett.* 100 (13) (2008) 136102.
- [19] Q. Wei, N. Li, N. Mara, M. Nastasi, A. Misra, Suppression of irradiation hardening in nanoscale V/Ag multilayers, *Acta Mater.* 59 (16) (2011) 6331–6340.
- [20] Q. Su, B. Cui, M.A. Kirk, M. Nastasi, In-situ observation of radiation damage in nano-structured amorphous SiOC/crystalline Fe composite, *Scr. Mater.* 113 (2016) 79–83.
- [21] Q. Su, F. Wang, B. Cui, M.A. Kirk, M. Nastasi, Temperature-dependent ion-beam mixing in amorphous SiOC/crystalline Fe composite, *Mater. Res. Lett.* 4 (4) (2016) 198–203. <http://www.tandfonline.com/doi/abs/10.1080/21663831.2016.1174164>.
- [22] I.-S. Kim, J. Hunn, N. Hashimoto, D. Larson, P. Maziasz, K. Miyahara, E. Lee, Defect and void evolution in oxide dispersion strengthened ferritic steels under 3.2 MeV Fe⁺ ion irradiation with simultaneous helium injection, *J. Nucl. Mater.* 280 (3) (2000) 264–274.
- [23] H. Oka, M. Watanabe, H. Kinoshita, T. Shibayama, N. Hashimoto, S. Ohnuki, S. Yamashita, S. Ohtsuka, In situ observation of damage structure in ODS austenitic steel during electron irradiation, *J. Nucl. Mater.* 417 (1) (2011) 279–282.
- [24] T. Allen, J. Gan, J. Cole, S. Ukai, S. Shutthanandan, S. Thevuthasan, The stability of 9Cr-ODS oxide particles under heavy-ion irradiation, *Nucl. Sci. Eng.* 151 (3) (2005) 305–312.
- [25] M. Lescoat, J. Ribis, A. Gentils, O. Kaitasov, Y. De Carlan, A. Legris, In situ TEM study of the stability of nano-oxides in ODS steels under ion-irradiation, *J. Nucl. Mater.* 428 (1) (2012) 176–182.
- [26] G. Hammersley, L.A. Hackel, F. Harris, Surface prestressing to improve fatigue strength of components by laser shot peening, *Opt. Lasers Eng.* 34 (4) (2000) 327–337.
- [27] O. Hatamleh, A comprehensive investigation on the effects of laser and shot peening on fatigue crack growth in friction stir welded AA 2195 joints, *Int. J. Fatigue* 31 (5) (2009) 974–988.
- [28] R.A. Brockman, W.R. Braisted, S.E. Olson, R.D. Tenaglia, A.H. Clauer, K. Langer, M.J. Shepard, Prediction and characterization of residual stresses from laser shock peening, *Int. J. Fatigue* 36 (1) (2012) 96–108.
- [29] R. Voothaluru, C.R. Liu, G.J. Cheng, Finite element analysis of the variation in residual stress distribution in laser shock peening of steels, *J. Manuf. Sci. Eng.* 134 (6) (2012) 061010.
- [30] Y. Al-Obaid, The effect of shot peening on stress corrosion cracking behaviour of 2205-duplex stainless steel, *Eng. Fract. Mech.* 51 (1) (1995) 19–25.
- [31] P.P. Shukla, P.T. Swanson, C.J. Page, Laser shock peening and mechanical shot peening processes applicable for the surface treatment of technical grade ceramics: a review, *Proc. Institution Mech. Eng. Part B J. Eng. Manuf.* 228 (5) (2014) 639–652.
- [32] S.R. Mannava, A.E. McDaniel, W.D. Cowie, H. Halila, J.E. Rhoda, J.E. Gutknecht, Laser Shock Peened Gas Turbine Engine Fan Blade Edges, General Electric Company, 1997.
- [33] R.L. Yeaton, Method and Apparatus for Laser Shock Peening, General Electric Company, 1998.
- [34] Y. Sano, M. Obata, T. Kubo, N. Mukai, M. Yoda, K. Masaki, Y. Ochi, Retardation of crack initiation and growth in austenitic stainless steels by laser peening without protective coating, *Mater. Sci. Eng. A* 417 (1) (2006) 334–340.
- [35] J. Lu, K. Luo, D. Yang, X. Cheng, J. Hu, F. Dai, H. Qi, L. Zhang, J. Zhong, Q. Wang, Effects of laser peening on stress corrosion cracking (SCC) of ANSI 304 austenitic stainless steel, *Corros. Sci.* 60 (2012) 145–152.
- [36] B. Cui, Q. Lu, D. Li, Q. Su, C. Zhang, Y. Lu, M. Nastasi, Laser shock peening of oxide-dispersion-strengthened austenitic stainless steels, *Trans. Am. Nucl. Soc.* 112 (2015) 292–293.
- [37] J. Lu, K. Luo, Y. Zhang, G. Sun, Y. Gu, J. Zhou, X. Ren, X. Zhang, L. Zhang, K. Chen, Grain refinement mechanism of multiple laser shock processing impacts on

- ANSI 304 stainless steel, *Acta Mater.* 58 (16) (2010) 5354–5362.
- [38] H. Ding, Y.C. Shin, Dislocation density-based modeling of subsurface grain refinement with laser-induced shock compression, *Comput. Mater. Sci.* 53 (1) (2012) 79–88.
- [39] C. Ye, Y. Liao, S. Suslov, D. Lin, G.J. Cheng, Ultrahigh dense and gradient nanoprecipitates generated by warm laser shock peening for combination of high strength and ductility, *Mater. Sci. Eng. A* 609 (2014) 195–203.
- [40] B. Mordyuk, Y.V. Milman, M. Iefimov, G. Prokopenko, V. Silberschmidt, M. Danylenko, A. Kotko, Characterization of ultrasonically peened and laser-shock peened surface layers of AISI 321 stainless steel, *Surf. Coatings Technol.* 202 (19) (2008) 4875–4883.
- [41] P. Peyre, X. Scherpereel, L. Berthe, C. Carboni, R. Fabbro, G. Beranger, C. Lemaitre, Surface modifications induced in 316L steel by laser peening and shot-peening, *Influ. pitting Corros. Resist. Mater. Sci. Eng. A* 280 (2) (2000) 294–302.
- [42] F. Wang, C. Zhang, Y. Lu, M. Nastasi, B. Cui, Laser shock processing of polycrystalline alumina ceramics, *J. Am. Ceram. Soc.* 100 (3) (2017) 911–919. <http://onlinelibrary.wiley.com/doi/10.1111/jace.14630/full>.
- [43] J.F. Ziegler, Stopping of energetic light ions in elemental matter, *J. Appl. Phys.* 85 (3) (1999) 1249–1272.
- [44] M. Briceño, J. Fenske, M. Dadfarnia, P. Sofronis, I.M. Robertson, Effect of ion irradiation-produced defects on the mobility of dislocations in 304 stainless steel, *J. Nucl. Mater.* 409 (1) (2011) 18–26.
- [45] M.L. Jenkins, M.A. Kirk, Characterisation of Radiation Damage by Transmission Electron Microscopy, Institute of Physics Publishing, Bristol, 2000.
- [46] R. Schramm, R. Reed, Stacking fault energies of seven commercial austenitic stainless steels, *Metall. Trans. A* 6 (7) (1975) 1345–1351.
- [47] D. Hull, D.J. Bacon, Introduction to Dislocations, Elsevier, 2011.
- [48] G. Cheng, M. Shehadeh, Dislocation behavior in silicon crystal induced by laser shock peening: a multiscale simulation approach, *Scr. Mater.* 53 (9) (2005) 1013–1018.
- [49] Z. Shen, R. Wagoner, W. Clark, Dislocation pile-up and grain boundary interactions in 304 stainless steel, *Scr. Metall.* 20 (6) (1986) 921–926.
- [50] Y. Hu, Z. Yao, J. Hu, 3-D FEM simulation of laser shock processing, *Surf. Coatings Technol.* 201 (3) (2006) 1426–1435.
- [51] Z. Zhou, A.S. Gill, D. Qian, S. Mannava, K. Langer, Y. Wen, V.K. Vasudevan, A finite element study of thermal relaxation of residual stress in laser shock peened IN718 superalloy, *Int. J. Impact Eng.* 38 (7) (2011) 590–596.
- [52] M. Suzuki, A. Fujimura, A. Sato, J. Nagakawa, N. Yamamoto, H. Shiraishi, In situ deformation of proton-irradiated metals, *Ultramicroscopy* 39 (1) (1991) 92–99.
- [53] Z. Jiao, J.T. Busby, G.S. Was, Deformation microstructure of proton-irradiated stainless steels, *J. Nucl. Mater.* 361 (2–3) (2007) 218–227.
- [54] G. Lucas, The evolution of mechanical property change in irradiated austenitic stainless steels, *J. Nucl. Mater.* 206 (2–3) (1993) 287–305.
- [55] R. Carter, M. Atzmon, G. Was, S. Bruegger, MRS Proceedings, in: *Deformation Mechanisms in a Proton-irradiated Austenitic Stainless Steel*, Cambridge Univ Press, 1994, p. 171.
- [56] M. Kirk, X. Yi, M. Jenkins, Characterization of irradiation defect structures and densities by transmission electron microscopy, *J. Mater. Res.* 30 (09) (2015) 1195–1201.
- [57] S. Zinkle, P. Maziasz, R. Stoller, Dose dependence of the microstructural evolution in neutron-irradiated austenitic stainless steel, *J. Nucl. Mater.* 206 (2) (1993) 266–286.
- [58] K. Urban, A. Seeger, Radiation-induced diffusion of point-defects during low-temperature electron irradiation, *Philos. Mag.* 30 (6) (1974) 1395–1418.
- [59] N. Soneda, T. Diaz de La Rubia, Migration kinetics of the self-interstitial atom and its clusters in bcc Fe, *Philos. Mag. A* 81 (2) (2001) 331–343.
- [60] D. Chen, J. Wang, T. Chen, L. Shao, Defect annihilation at grain boundaries in alpha-Fe, *Sci. Rep.* 3 (2013).
- [61] P. Heald, The preferential trapping of interstitials at dislocations, *Philos. Mag.* 31 (3) (1975) 551–558.
- [62] D. Rodney, G. Martin, Y. Bréchet, Irradiation hardening by interstitial loops: atomistic study and micromechanical model, *Mater. Sci. Eng. A* 309 (2001) 198–202.
- [63] B. Singh, A. Foreman, H. Trinkaus, Radiation hardening revisited: role of intracascade clustering, *J. Nucl. Mater.* 249 (2) (1997) 103–115.
- [64] N. Ghoniem, S.-H. Tong, B. Singh, L. Sun, On dislocation interaction with radiation-induced defect clusters and plastic flow localization in fcc metals, *Philos. Mag. A* 81 (11) (2001) 2743–2764.
- [65] M. Victoria, N. Baluc, C. Bailat, Y. Dai, M. Luppó, R. Schaublin, B. Singh, The microstructure and associated tensile properties of irradiated fcc and bcc metals, *J. Nucl. Mater.* 276 (1) (2000) 114–122.
- [66] H. Trinkaus, B. Singh, A. Foreman, Mechanisms for decoration of dislocations by small dislocation loops under cascade damage conditions, *J. Nucl. Mater.* 249 (2) (1997) 91–102.
- [67] Y. Matsukawa, G.S. Liu, In situ TEM study on elastic interaction between a prismatic loop and a gliding dislocation, *J. Nucl. Mater.* 425 (1) (2012) 54–59.
- [68] J. Robach, I. Robertson, B. Wirth, A. Arsenlis, In-situ transmission electron microscopy observations and molecular dynamics simulations of dislocation-defect interactions in ion-irradiated copper, *Philos. Mag.* 83 (8) (2003) 955–967.
- [69] A. Brailsford, R. Bullough, The theory of sink strengths, philosophical transactions of the royal society of London a: mathematical, *Phys. Eng. Sci.* 302 (1465) (1981) 87–137.
- [70] L. Mansur, Theory and experimental background on dimensional changes in irradiated alloys, *J. Nucl. Mater.* 216 (1994) 97–123.
- [71] S.J. Zinkle, L.L. Snead, Designing radiation resistance in materials for fusion energy, *Annu. Rev. Mater. Res.* 44 (2014) 241–267.
- [72] X.-M. Bai, B.P. Uberuaga, The influence of grain boundaries on radiation-induced point defect production in materials: a review of atomistic studies, *JOM* 65 (3) (2013) 360–373.
- [73] M.A. Tschopp, K. Solanki, F. Gao, X. Sun, M.A. Khaleel, M. Horstemeyer, Probing grain boundary sink strength at the nanoscale: energetics and length scales of vacancy and interstitial absorption by grain boundaries in α -Fe, *Phys. Rev. B* 85 (6) (2012) 064108.
- [74] A.H. King, D. Smith, On the mechanisms of point-defect absorption by grain and twin boundaries, *Philos. Mag. A* 42 (4) (1980) 495–512.
- [75] M. Mendelev, A. King, The interactions of self-interstitials with twin boundaries, *Philos. Mag.* 93 (10–12) (2013) 1268–1278.
- [76] N. Li, J. Wang, Y. Wang, Y. Serruys, M. Nastasi, A. Misra, Incoherent twin boundary migration induced by ion irradiation in Cu, *J. Appl. Phys.* 113 (2) (2013) 023508.
- [77] I. Beyerlein, A. Caro, M. Demkowicz, N. Mara, A. Misra, B. Uberuaga, Radiation damage tolerant nanomaterials, *Mater. Today* 16 (11) (2013) 443–449.